Absorption cross sections and Auger recombination lifetimes in inverted core-shell nanocrystals: Implications for lasing performance

J. Nanda,[a] S. A. Ivanov,[a] H. Htoon,[a] I. Bezel,[a] A. Piryatinski,[b] S. Tretiak,[b] and V. I. Klimov[a,c]
Los Alamos National Laboratory, Los Alamos, New Mexico 87545

(Received 23 June 2005; accepted 22 December 2005; published online 9 February 2006)

We study inverted core-shell nanocrystals (NCs), in which a core of a wide-gap semiconductor (ZnSe) is overcoated with a shell of a narrower gap material (CdSe). Depending on the core radius and the shell thickness, these NCs can exhibit either type-I or type-II behavior. We show that these heterostructures can be used to significantly increase the absorption cross sections and simultaneously decrease the efficiency of Auger recombination compared to monocomponent CdSe NCs emitting at the same wavelength. These properties enhance the lasing performance of inverted core-shell structures and allow, in particular, efficient amplified spontaneous emission in the range of blue colors. © *2006 American Institute of Physics*. [DOI: 10.1063/1.2168032]

I. INTRODUCTION

Colloidal semiconductor nanocrystals (NCs) have been a subject of intense research due to both their size-controlled electronic and optical properties[1–3] and large technological potential for applications in such areas as biolabeling,[4,5] photovoltaics,[6,7] light-emitting diodes,[8–11] nonlinear optics,[12] and lasing.[13–16] By exploiting the effects of quantum confinement, one can continuously tune the NC energy gap by hundreds of meV, which directly translates into a wide-range tunability of emission and absorption spectra.[17] While being a powerful tool for controlling spectral responses of NCs, the quantum-size effect has a limited applicability for engineering the strength of optical transitions and dynamical and nonlinear (electronic or optical) responses of nanostructures. For example, in CdSe NCs single-exciton, radiative-decay dynamics are almost size independent[18] because of a very weak dependence of the electron-hole (*e-h*) overlap integral on nanoparticle dimensions. Furthermore, in some cases the change in the NC dimensions required to produce a certain spectral response (e.g., a particular emission wavelength) can unfavorably affect some other important parameters of NCs. For example, in order to obtain large blueshifts of emission spectra with respect to the bulk energy gap, one needs to use NCs of small sizes. However, a decrease in the NC size leads to such adverse effects such as decreased absorption cross sections,[19] smaller nonlinear optical susceptibilities,[20] increased nonradiative carrier losses associated with surface trapping,[21] and increased efficiency of nonradiative multiexciton Auger recombination.[22]

One approach to decoupling the control of emission wavelengths from the control of such parameters as absorption cross sections and Auger recombination times involves the use of elongated NCs (quantum rods).[23,24] In a quantum rod, the confinement energy is primarily determined by its dimension along the short axis, while the absorption cross sections and Auger decay constants are defined by the rod volume (i.e., by the rod length for a constant cross-sectional size). Using these properties of rods, one can engineer elongated nanoparticles that show significantly increased absorption cross sections and reduced Auger rates compared to spherical NCs emitting at the same wavelength.[23] This capability further allows one to greatly reduce an optical-gain threshold and a threshold for amplified spontaneous emission (ASE).[24]

In this paper, we describe another approach for manipulating the spectral properties and dynamics of NCs by utilizing "inverted" core/shell heteronanostructures. Specifically, we synthesize and study hetero-NCs, in which a core of a wide-gap semiconductor (ZnSe) is overcoated with a shell of a narrower gap material (CdSe). Compared to monocomponent CdSe NCs or traditional "noninverted" hetero-NCs [such as CdSe(core)/ZnS(shell)[25] or CdSe(core)/CdS(shell)[26]], these "inverted" NCs provide capabilities for controlling functionalities by a direct control of the distribution of electron and hole wave functions and the *e-h* overlap integral.[27,28] Specifically, by increasing the thickness of the NC shell (for a fixed NC core size), one can continuously tune the carrier localization regime from type I for thin shells (both electron and hole wave functions are distributed over an entire volume of the NC) to type II for intermediate shells (electron and hole are spatially separated between the shell and the core) and finally back to type I for thick shells (electron and hole colocalize in the shell) (Fig. 1).[28,29] In the present work, we concentrate on the comparative analysis of absorption cross sections and Auger recombination time constants in inverted ZnSe/CdSe hetero-NCs (see Sec. II for sample description) and monocomponent spherical (quantum dots) and elongated (quantum rods) CdSe NCs. To directly measure the absorption cross sections of hetero-NCs, we apply a technique that is based on absorption saturation measurements (Sec. III). After quantifying absorption cross sections of hetero-NCs, we perform measurements of transient absorption (TA) dynamics in single- and double-exciton

[a]C-PCS, Chemistry Division.
[b]T-12, Theoretical Division.
[c]Author to whom correspondence should be addressed; electronic mail: klimov@lanl.gov

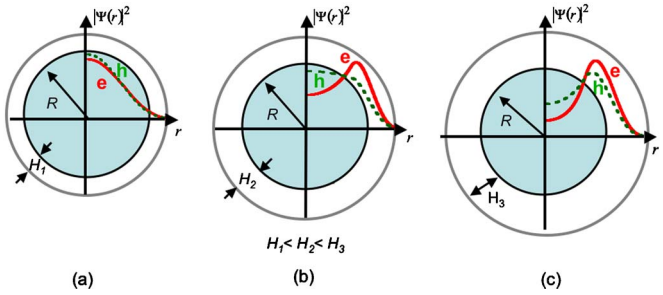

FIG. 1. (Color online) Calculated spatial distributions of electron (solid line) and hole (dashed line) wave functions in ZnSe/CdSe "inverted" core/shell NCs with a fixed ZnSe core radius (R=1.5 nm) and three different CdSe shell thicknesses (H=0.45 nm) 0.45, 1.3, and 1.9 nm) that correspond to three different localization regimes. (a) Thin shell: an electron and a hole reside primarily in the core [type-I (core/core) regime]. (b) Intermediate shell: the electron is preferentially localized in the shell while the hole still stays primarily in the core [type-II (core/shell) regime]. (c) Thick shell: both the electron and the hole are localized primarily in the shell [type-I (shell/shell) regime].

(biexciton) pump regimes that allow us to derive biexciton Auger recombination time constants (Sec. IV). The analysis of parameters derived for hetero-NCs and those measured previously for quantum dots[13] and quantum rods[23] indicates that while rods provide increased absorption cross sections and reduced Auger recombination rates compared to dots on the orange-to-red end of the optical spectrum, the inverted hetero-NCs provide a similar improvement in the "difficult" range of yellow, green, and blue colors that correspond to the regime of strong quantum confinement. As discussed in Sec. V (Conclusions), these properties of inverted core-shell structures are advantageous for lasing applications and allow, in particular, demonstration of light amplification in the range of blue colors.

II. SAMPLES: FABRICATION AND OPTICAL PROPERTIES OF INVERTED CORE/SHELL NANOCRYSTALS

The preparation of inverted core/shell ZnSe/CdSe hetero-NCs is a two-step procedure, in which we initially synthesize ZnSe seed particles and then overcoat them with a CdSe shell. The synthesis of ZnSe NCs passivated with hexadecylamine (HDA) and trioctylphosphine (TOP) is conducted according to the published route.[30] To perform overcoating with CdSe, the ZnSe NC growth solution in HDA is introduced into degassed TOPO at 140–150 °C. Following the injection and temperature stabilization, the solution of CdSe precursors (dimethylcadmium and TOPSe) in TOP is added to the reaction mixture. The amount of injected cadmium is determined by the desired shell thickness, but the Cd:Se ratio is always kept between 1:1 and 1:2. The thickness of the CdSe shell is qualitatively monitored by noting the changes in the position of the photoluminescence (PL) band [Fig. 2(a)]. After the addition of cadmium and selenium precursors, the reaction mixture is stirred for 24–48 hours (the annealing stage), which is essential for obtaining high PL quantum yields of the synthesized ZnSe/CdSe core/shell NCs. A further increase in the PL quantum yield of blue and green emitting NCs can be achieved via additional overcoating of a ZnSe/CdSe nanostructure with ZnS, which results in

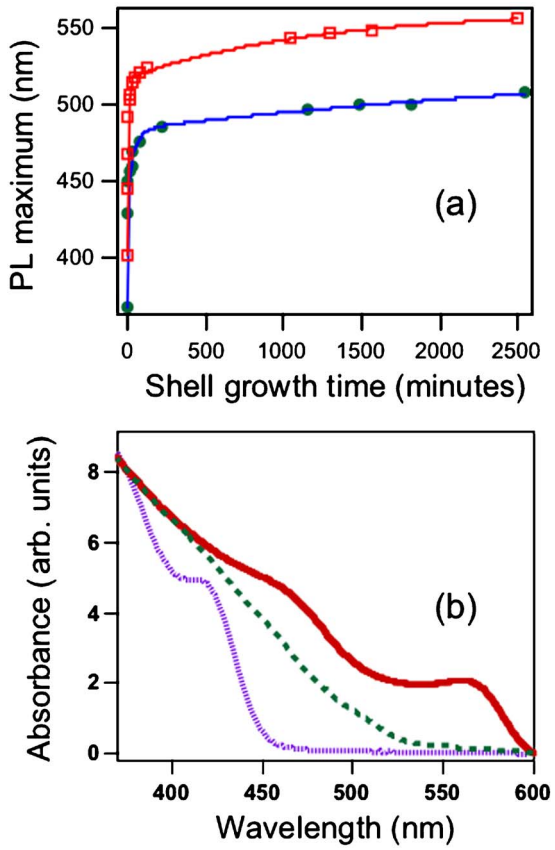

FIG. 2. (Color online) Evolution of the PL maximum with time during the growth of the CdSe shell leading to the formation of type-II (solid circle) and type-I (open square) structures, respectively. The ZnSe core radius is ca. 1.5 nm. The two dependences shown in the plot are obtained for two different relative amounts of the Cd and Se precursors compared to ZnSe cores. (b) Optical absorption spectra of ZnSe/CdSe inverted core-shell NCs with a fixed core radius (ca. 1.5 nm) and three different shell thicknesses that correspond to the three different localization regimes illustrated in Fig. 1: type I (core/core) (dotted line), type II (core/shell) (dashed line), and type I (shell/shell) (solid line).

a double-shell ZnSe/CdSe/ZnS hetero-NC. For ZnS overcoating, ZnS precursors (diethylzinc and hexamethyldisilathiane in the 1:1 ratio) in TOP are added directly into ZnSe/CdSe growth solution at 140–160 °C, and the mixture is annealed for 24 hours. While providing improved emission efficiencies, the ZnS layer does not significantly affect the spatial distribution of electron and hole wave functions (as indicated by the comparison of PL and absorption spectra of NCs with and without ZnS overcoating). Therefore, in the discussion of spectroscopic results below we do not specify whether they are obtained for single-or double-shell structures.

Formation of the core-shell structure is confirmed by the results from transmission electron microscopy (TEM), x-ray-diffraction, and x-ray photoelectron spectroscopy studies (see supplemental information in Ref. 29). The fabricated NCs produce efficient emission (absolute quantum yields are up to 60–80%) that is tunable from 430 to 600 nm. The emission line widths are from 30 to 40 nm indicating good monodispersity of synthesized hetero-NCs.

In Fig. 2(b) we display the optical absorption spectra of three core-shell samples having approximately the same

ZnSe core radius (R) of 15 Å (as determined from TEM studies) and different CdSe shell thicknesses (H) that correspond to emission wavelengths from 440 to 552 nm. Electronic structure calculations based on the effective-mass approximation (see supplemental material in Ref. 29) indicate that this range of emission wavelengths span all three possible localization regimes discussed in the Introduction (see also Fig. 1). The change in carrier localization is well manifested in the absorption spectra displayed in Fig. 2(b). For ZnSe NCs, the $1S$ absorption maximum occurs at 355 nm. After the cadmium and selenium precursors are added to the ZnSe cores, the $1S$ peak rapidly shifts to 420–430 nm, which occurs because of the increase in the effective volume of the exciton. This exciton, however, remains "spatially direct" (type-I localization regime with both carriers distributed over the entire hetero-NC volume), as indicated by the presence of a well-defined $1S$ absorption maximum [dotted line in Fig. 2(b)]. A further increase in the shell thickness leads to the smearing out of the $1S$ absorption peak [dashed line in Fig. 2(b)]. This change is not accompanied by a broadening of the PL band, indicating that the changes observed in the absorption spectra are not due to an increase in sample polydispersity but rather result from the transition to a type-II *spatially indirect exciton* that is characterized by a reduced oscillator strength. As the shell thickness is further increased, we observe a gradual restoration of the sharp, band-edge absorption peak [solid line in Fig. 2(b)], indicating a transition to type-I localization (both carriers reside primarily in the shell) characterized by an increased *e-h* overlap. From a comparative analysis of the PL and the second derivative absorption spectra[29] and from the radiative decay dynamics,[28] we conclude that the transitions between different localization regimes occur at emission wavelengths of ~460 nm (type I to type II) and ~510 nm (type II to type I).

For the remainder of this article, we concentrate on five core-shell NC samples with emission wavelengths of 478 (sample 1), 507 (sample 2), 522 (sample 3), 549 (sample 4), and 552 nm (sample 5). For all of these samples, the electron is expected to be localized in the shell, while a hole is localized either primarily in the core (samples 1 and 2) or in the shell (samples 3, 4, and 5). Thus, samples 1 and 2 are characterized by type-II localization, while samples 3, 4, and 5 correspond to type-I localization. Because of the small electron mass, the high-energy shift of the lowest optical transitions (the "emitting" transition) with respect to the bulk CdSe energy gap is dominated by the electron confinement energy. For all of the samples, the electron is primarily confined in the shell; therefore, the shell thickness is the main factor that determines the emission wavelength. Furthermore, the changes in hole localization during the transition from the type I to the type-II regime are not expected to significantly affect the overall shell-thickness dependence of the emission wavelength.

III. ABSORPTION CROSS SECTIONS

In this work we analyze absorption cross section (σ_a) in the range of spectral energies, $\hbar\omega$, that are much higher than the energy gap. As shown in Refs. 19 and 24, in this case the absorption cross section of both spherical and elongated monocomponent nanoparticles is directly proportional to the NC volume (V): $\sigma_a(\hbar\omega)=(n_b/n)\alpha_b(\hbar\omega)|f(\hbar\omega)|^2V$, in which α_b and n_b are the absorption coefficient and the refractive index of the bulk semiconductor, respectively, n is the refractive index of the NC sample (for dilute samples, n is close to the refractive index of the matrix/solvent), and f is the local-field factor that accounts for the difference in the electric field inside and outside of the NC.

One may expect that for inverted hetero-NCs, the absorption cross section at high spectral energies should also be simply proportional to the total volume of the heterostructure, as in the case of monocomponent NCs, because the excited-state electron and hole wave functions are distributed over the entire hetero-NC volume.[28,29] On the other hand, the emission wavelength of the hetero-NCs is determined by the energy of the transition that couples ground electron and hole states. The spatial distribution of wave functions for these states is a function of both core radius and shell width.[28,29] Specifically, in the case of the predominant localization of the electron in the shell, the confinement energy can be made large by reducing the shell thickness, while one can still maintain a large absorption cross section by increasing the core size and, hence, the total volume of the hetero-NC. Below, we show that by using inverted hetero-NCs, we can indeed increase the absorption cross section by more than an order of magnitude compared to monocomponent CdSe NCs while maintaining the same confinement energy (measured from the position of the emission band).

In order to quantify absorption cross sections of hetero-NCs, we apply a nonlinear optical method utilizing absorption saturation measurements performed using a TA experiment. In our experimental configuration, the samples are excited using 100 fs, frequency-doubled pulses from an amplified Ti:sapphire laser (3.1 eV photon energy). Pump-induced absorption changes ($\Delta\alpha$) are probed using variably delayed pulses of a femtosecond white-light continuum. This system provides accuracy up to 10^{-4}–10^{-5} in differential transition (for experimental details see Ref. 31).

In II–VI NCs, the density of valence-band states is significantly higher than the density of conduction-band states, which is a combined result of a large hole effective mass and a complex multisubband structure of the valence band. Therefore, state-filling-induced TA signals are dominated by populations of electron states.[19,32] Specifically, the pump-induced absorption change ($\Delta\alpha$) at the position of the lowest absorption feature normalized by linear absorption (α_0) is proportional to the number of electrons occupying the lowest conduction-band quantized state averaged over a NC ensemble and divided by the state degeneracy.[19,33] The lowest electron state in ZnSe/CdSe NCs is twofold spin degenerate; therefore, the normalized absorption change can be expressed by the following expression:[19] $|\Delta\alpha|/\alpha_0=\langle n_{1S}\rangle$, in which $\langle n_{1S}\rangle$ is the average occupation number of the $1S$ state with a certain spin projection. Assuming a Poissonian distribution of NC populations, we obtain[33]

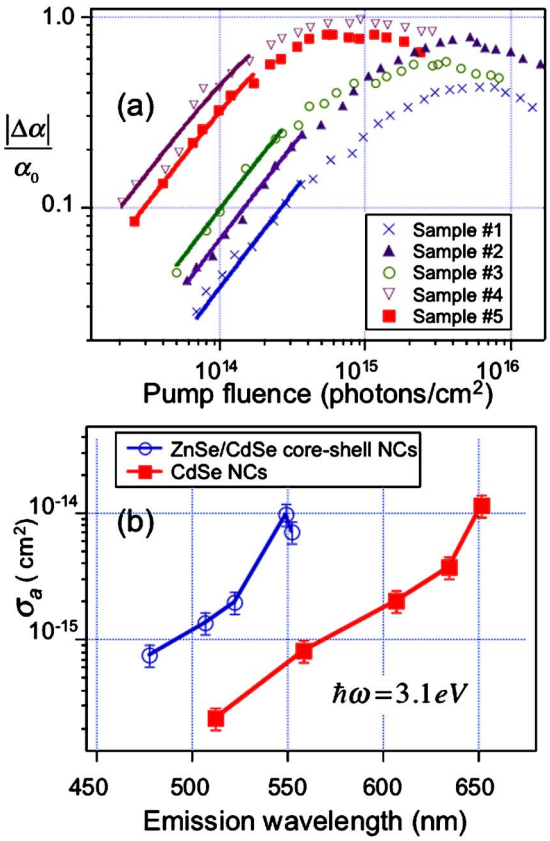

FIG. 3. (Color online) (a) Pump dependence of the 1*S* absorption bleaching for ZnSe/CdSe inverted core/shell NCs (samples 1–5) measured at 2 ps after excitation (pump photon energy is 3.1 eV). The solid lines are the fits to Eq. (3) used to derive absorption cross sections. (b) Absorption cross sections at 3.1 eV plotted as a function of emission wavelength for monocomponent CdSe quantum dots (solid squares) and ZnSe/CdSe inverted core/shell NCs (open circles).

$$\left.\frac{|\Delta\alpha|}{\alpha_0}\right|_{1S} = \left[1 - e^{-\langle N\rangle}\left(1 + \frac{\langle N\rangle}{2}\right)\right], \tag{1}$$

where $\langle N\rangle$ is the average number of *e-h* pairs per NC. In the case for which both the pump pulse duration and the delay time after excitation are much shorter than the recombination time constant, $\langle N\rangle$ is directly proportional to pump fluence (j_p) and can be expressed by the following expression:

$$\langle N\rangle = j_p \sigma_a(\hbar\omega_p), \tag{2}$$

where $\sigma_a(\hbar\omega_p)$ is the absorption cross section of the NC at the pump spectral energy (j_p is presented in terms of the number of photons per cm^2 per pulse). By combining Eqs. (1) and (2), we obtain the following expression for normalized absorption changes, which we use in the analysis of our experimental data:

$$\left.\frac{|\Delta\alpha|}{\alpha_0}\right|_{1S} = \left\{1 - e^{-j_p\sigma_a(\hbar\omega_p)}\left(1 + \frac{j_p\sigma_a(\hbar\omega_p)}{2}\right)\right\}. \tag{3}$$

Figure 3(a) displays $|\Delta\alpha|/\alpha_0$ as a function of pump fluence measured at a pump-probe delay (Δt) of 2 ps for core-shell samples 1–5. These data show initial linear growth followed by saturation, which is similar to the behavior observed experimentally for both monocomponent NCs and noninverted core-shell structures.[19,34,35] The saturation of the TA signal occurs because the maximum occupancy of the lowest electron state is limited by its degeneracy. Equation (3) predicts that the "saturated" value of $|\Delta\alpha|/\alpha_0$ is 1. Experimentally, however, we observe that while the saturation threshold is indeed close to 1 in samples with a thicker shell (emission at 552 and 549 nm), the samples with thinner shell show saturation at values below unity. This effect was previously observed for monocomponent CdSe NCs (Ref. 35) and was explained in terms of an additive contribution from photoinduced absorption (PA) that was attributed to carriers trapped at the NC interface. These previous studies also indicated that the effect of PA was more significant in smaller NCs that exhibited stronger confinement and were characterized by greater surface-to-volume ratios. A similar trend is observed for core-shell structures with thinner shells that have greater confinement energies and that show lower saturated bleaching values (i.e., a greater PA contribution). Another result of Ref. 35 is that PA is characterized by a certain excitation threshold and, therefore, its role at low pump intensity (specifically, below the $\Delta\alpha$ saturation threshold) is insignificant. All of these observations indicate that despite the fact that some of the core-shell samples show below unity saturated values of $|\Delta\alpha|/\alpha_0$, Eq. (3) can still be used to describe pump-induced absorption changes in the range of low pump intensities.

By fitting the experimental saturation curves in the range of small fluences to Eq. (3) [see Fig. 3(a)], we derive the absorption cross sections that are displayed in Fig. 3(b) as a function of the emission wavelength (open circles). In the same figures we also show the absorption cross sections of monocomponent CdSe NCs (solid squares). The comparison of these two sets of data indicate that inverted core/shell NCs have up to more than an order of magnitude higher absorption cross sections compared to monocomponent NCs emitting at the same wavelength. As was discussed in the beginning of this section, the large absorption cross sections in inverted core-shell structures at large spectral energies can occur simultaneously with a large, confinement-induced energy shift of the lowest optical transition because of a significant difference in the effective volume of the electronic excitation in the high-energy state (both an electron and a hole delocalized over the entire hetero-NC) and the ground state (electron is localized primarily in the shell for all structures shown in Fig. 3).

IV. AUGER RECOMBINATION OF BIEXCITONS

The effect of the transition from type-I to type-II carrier localization on single *e-h* pair (i.e., single exciton) recombination dynamics was studied in Ref. 28. It was observed that for samples with a fixed core radius and increasing shell thickness, a change in recombination dynamics directly correlates with the change in the *e-h* overlap integral, which is a behavior expected for relaxation due to radiative decay.

The decay of multiexcitons in NCs is, however, dominated not by radiative processes but by nonradiative Auger recombination,[22] in which the *e-h* recombination energy is transferred to a third carrier (an electron or a hole). Previous studies of spherical[22] and elongated[23] (quantum rods) CdSe

nanoparticles as well as PbSe spherical NCs (Ref. 7) indicate that in all of these systems Auger decay is extremely fast (picosecond time scales) and is characterized by time constants that scale proportionally to the NC volume (i.e., proportionally to the radius cubed in the case of spherical NCs). Because of this strong size dependence, small monocomponent NCs are characterized by the extremely fast multiexciton Auger recombination leading to a very short optical-gain lifetime.[36] Fast relaxation of the optical gain represents a major complication for achieving lasing in NC materials[13] and is a particularly severe problem in the range of large confinement energies (green-blue emission colors in the case of CdSe NCs) that correspond to small NC sizes. As discussed below, the use of inverted core-shell NCs allows us to significantly suppress the Auger recombination, which simplifies obtaining the ASE regime in the green-blue region of the optical spectrum.

Our approach relies on the fact that the Auger recombination is mediated by Coulomb electrostatic interactions. Hence, the Auger decay rate is determined not by the overlap of electron and hole wave functions but rather the spatial separation between interacting carriers. The rates of the Auger recombination in the inverted hetero-NC are not expected to be very sensitive to its internal structure (and the *e-h* overlap) but instead, should primarily be determined by the outer size of the hetero-NC (i.e., by its total volume). Based on the arguments similar to those made in the case of absorption cross sections (see previous section), one can expect that by using inverted core-shell NCs with "shell-localized" electrons, it should be possible to substantially suppress the Auger recombination while still maintaining strong quantum confinement.

To measure the Auger life times of two-exciton (biexciton) states (τ_2) in ZnSe/CdSe core-shell NCs, we use a TA experiment, in which we monitor the decay of the lowest (1*S*) bleaching feature at "low" and "high" pump intensities that correspond to initial NC populations $\langle N_0\rangle \ll 1$ and $1 < \langle N_0\rangle < 2$, respectively (the average number of initially photogenerated *e-h* pairs per NC, $\langle N_0\rangle$, was estimated using absorption cross sections derived in the previous section). To translate $\Delta\alpha$ dynamics into dynamics of NC average populations, we use absorption saturation curves similar to those shown in Fig. 3(a). Finally, we extract the biexciton dynamics using a subtractive procedure from Ref. 22.

The biexciton decay curves derived for three different core-shell samples (emission wavelengths of 507, 523, and 549 nm) are displayed in Fig. 4(a). One observation is that the biexciton life times (sub-100 ps time scale) are significantly shorter than the lifetime of the single-exciton states (>25 ns),[28] indicating that these two types of excitations decay via different relaxation mechanisms. The intrinsic decay of single excitons is dominated by radiative recombination. The rate of this process decreases as the emission wavelength changes from 522 to 478 nm (the range studied in this paper), because of the transition from type-I to type-II localization that is accompanied by the reduction of the *e-h* overlap integral.[28] The biexciton decay rates show the opposite trend, namely, the increase in the magnitude with decreasing wavelength. Both ultrashort sub-100 ps time constants and

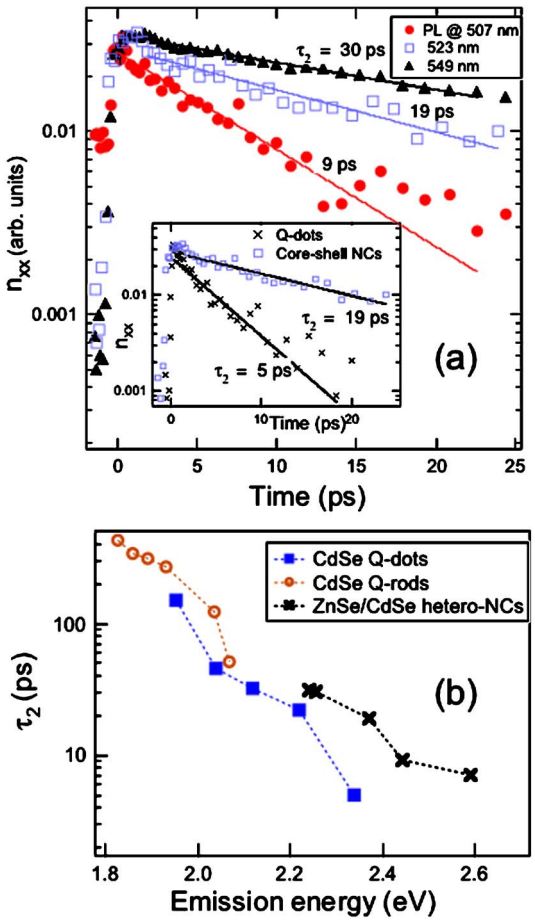

FIG. 4. (Color online) (a) Extracted Auger recombination dynamics of NC biexciton states, $n_{xx}(t)$, for three core-shell samples emitting at 507 nm (solid circles), 523 nm (open squares), and 549 nm (solid triangles). Inset: a comparison of the biexciton decay in monocomponent CdSe and heterostructured ZnSe/CdSe NCs emitting at 2.35 and 2.37 eV, respectively. (b) The dependence of the biexciton Auger life time on the emission wavelength for CdSe NCs (solid squares), CdSe quantum rods (open circles), and ZnSe/CdSe inverted core/shell heterostructures (crosses) (CdSe NCs have radii from 1.2 to 4.1 nm, while quantum rod samples have the same radius of 2.3 nm and different lengths from 22 to 44 nm).

the increase in the relaxation rate with increasing degree of quantum confinement (leading to shorter emission wavelengths) are typical for nonradiative Auger recombination, which dominates the biexciton decay in, e.g., monocomponent CdSe NCs.[22] The absolute rate of the Auger decay in inverted core-shell ZnSe/CdSe NCs is, however, significantly lower than in CdSe-core NCs emitting at the same wavelength (i.e., characterized by the same confinement energy). For example, CdSe quantum dots emitting at about 2.35 eV are characterized by τ_2 of approximately 5 ps, while in core-shell NCs emitting at ca. 2.37 eV, τ_2 is 19 ps, which is almost four times longer [see inset of Fig. 4(a)].

In Fig. 4(b), we plot the Auger recombination time constants for biexciton states of core-shell NCs with different shell thicknesses as a function of emission wavelength (crosses). These data are compared with time constants previously measured for CdSe quantum dots (solid squares)[22] and quantum rods (open circles).[23] From the plot in Fig. 4(b), one can see that quantum rods provide an increase in Auger life times compared to spherical nanoparticles in the red-

orange range of the optical spectrum that corresponds to relatively small confinement energies. As was discussed in Ref. 23, this increase occurs because of the larger rod volume that can be obtained by increasing the rod length without significantly affecting the emission energy (the latter is primarily controlled by the rod diameter[37]).

In addition to the nanoparticle volume, the efficiency of Auger recombination is also dependent on the NC surface area and, specifically, it increases with increasing surface-to-volume ratio.[23] Therefore, quantum rods do not provide suppression of Auger rates at the high spectral energies (strong quantum confinement) that correspond to small rod diameters and, hence, large surface-to-volume ratios. For example, the biexciton recombination time in quantum rods is approaching that of quantum dots at emission energy of approximately 2.1 eV [Fig. 4(b)].

The use of inverted core-shell NCs, on the other hand, allows us to significantly suppress the Auger recombination in the range of large confinement energies (green and blue emission colors). As illustrated in Fig. 4(b), core-shell hetero-NCs systematically show longer Auger time constants compared to monocomponent quantum dots for emission energies greater than ca. 2.2 eV. As was discussed in the beginning of this section, the suppression of Auger decay occurs because inverted hetero-NCs allow us to obtain a large separation between interacting carriers (defined by the outer NC size) simultaneously with large confinement energies (determined by the shell thickness). Furthermore, the decrease in the shell thickness required to produce strong confinement does not lead to a significant increase of the interfacial surface area and does not enhance the Auger recombination via the factor associated with the surface-to-volume ratio.

V. CONCLUSIONS

We report on the fabrication and spectroscopic studies of inverted core-shell hetero-NCs, in which a core of a wide-gap semiconductor (ZnSe) is overcoated with a shell of a narrower gap material (CdSe). While CdSe and ZnSe are characterized by type-I energy offsets in the bulk form, ZnSe/CdSe core/shell structures can exhibit either type-I or type-II behavior depending on the core radius and the shell thickness. Specifically, for NCs with a fixed core radius and progressively increasing shell thickness, carrier localization can be continuously tuned from type I (electron and hole are delocalized over the entire NC) to type II (the electron is localized mostly in the shell while the hole resides primarily in the core) and then back to type-I (both electron and hole are primarily localized in the shell) regimes. Here, we have studied core-shell structures, in which an electron and a hole are either separated between the shell and the core, respectively, or are both primarily located in the shell (i.e., structures with "shell-localized" electrons). We show that these structures can be used to significantly increase the absorption cross sections and to decrease the efficiency of Auger recombination in the range of green and blue emission colors that correspond to large confinement energies. These properties of inverted NCs arise from the fact that while both absorption cross sections and Auger recombination rates are primarily determined by the total hetero-NC volume, the emission energy is defined mostly by the NC shell thickness.

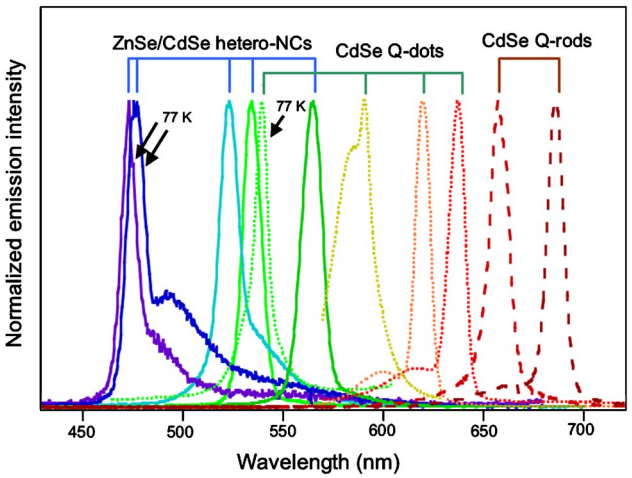

FIG. 5. (Color online) Amplified spontaneous emission tunable from red to blue using CdSe quantum rods (red emission color), CdSe quantum dots (red through green emission colors), and ZnSe/CdSe inverted core/shell NCs (green through blue emission colors). These spectra are obtained either at room temperature or at 77 K (labeled). All samples were excited at 3.1 eV using frequency-doubled 100 fs pulses from an amplified Ti:sapphire laser.

The increased absorption cross sections and decreased Auger recombination efficiency are beneficial for lasing applications. Specifically, these properties of inverted core-shell structures allow the extension of the spectral range accessible in the lasing regime to shorter wavelengths. Room-temperature ASE was demonstrated using CdSe quantum dots and quantum rods in the range of red, orange, and yellow colors (637–590 nm, dashed and dotted lines in Fig. 5).[13,16,20,36,38] The ASE range can be extended to the green (ca. 540 nm) using quantum dots cooled to liquid-nitrogen temperature (dashed-dotted line in Fig. 5). Observation of the ASE at shorter wavelengths using quantum dot samples is severely complicated by a rapid decrease in both the Auger recombination time and absorption cross sections. On the other hand, as was demonstrated in Ref. 29, inverted hetero-NCs can be used to produce optical gain and ASE tunable in the range of green and blue colors (565–475 nm, solid lines in Fig. 5). In addition to increased absorption cross sections and reduced rates of the Auger decay, the superior ASE performance of inverted core-shell structures compared to monocomponent NCs is also a consequence of reduced excited-state absorption resulting from exciton-exciton repulsion that can be realized in the type-II localization regime.[29] As illustrated in Fig. 5, using CdSe-based colloidal nanostructures prepared as quantum dots, quantum rods, or inverted core-shell NCs one can achieve a continuous coverage of the entire visible spectral range in the ASE regime.

ACKNOWLEDGMENTS

This work was supported by Los Alamos LDRD Funds and the Chemical Sciences, Biosciences, and Geosciences Division of the Office of Basic Energy Sciences, Office of Science, U.S. Department of Energy.

[1]S. V. Gaponenko, *Optical Properties of Semiconductor Nanocrystals* (Cambridge University Press, Cambridge, 1999).
[2]V. I. Klimov, *Semiconductor and Metal Nanocrystals: Synthesis and Electronic and Optical Properties* (Marcel Dekker, New York, 2004).
[3]Al. L. Efros, D. J. Lockwood, and L. Tsybeskov, *Semiconductor Nanocrystals: From Basic Principles to Application* (Kluwer Academic, Dordrecht, 2003).
[4]D. Larson, W. Zipfel, R. Williams, M. Bruchez, S. Clark, F. W. Wise, and W. W. Webb, Science **300**, 1434 (2003).
[5]A. P. Alivisatos, Nat. Biotechnol. **22**, 47 (2004).
[6]W. U. Huynh, J. J. Dittmer, and A. P. Alivisatos, Science **295**, 2425 (2002).
[7]R. D. Schaller and V. I. Klimov, Phys. Rev. Lett. **92**, 186601 (2004).
[8]W. S. Coe, W.-K. Woo, M. G. Bawendi, and V. Bulovic, Nature (London) **420**, 800 (2002).
[9]V. L. Colvin, M. C. Schlamp, and A. P. Alivisatos, Nature (London) **370**, 354 (1994).
[10]B. O. Dabbousi, M. G. Bawendi, O. Onitsuka, and M. F. Rubner, Appl. Phys. Lett. **66**, 1316 (1995).
[11]N. Tessler, V. Medvedev, M. Kazes, S. Kan, and U. Banin, Science **295**, 1506 (2002).
[12]B. Kraabel, A. Malko, J. Hollingsworth, and V. I. Klimov, Appl. Phys. Lett. **78**, 1814 (2001).
[13]V. I. Klimov, A. Mikhailovsky, S. Xu, A. Malko, J. Hollingsworth, C. A. Leatherdale, and M. G. Bawendi, Science **290**, 314 (2000).
[14]A. V. Malko, A. A. Mikhailovsky, M. A. Petruska, J. A. Hollingsworth, H. Htoon, M. G. Bawendi, and V. I. Klimov, Appl. Phys. Lett. **81**, 1303 (2002).
[15]H.-J. Eisler, V. C. Sundar, M. G. Bawendi, M. Walsh, H. I. Smith, and V. I. Klimov, Appl. Phys. Lett. **80**, 4614 (2002).
[16]M. Kazes, D. Y. Lewis, Y. Ebenstein, T. Mokari, and U. Banin, Adv. Mater. (Weinheim, Ger.) **14**, 317 (2002).
[17]C. B. Murray, D. J. Norris, and M. G. Bawendi, J. Am. Chem. Soc. **115**, 8706 (1993).
[18]S. A. Crooker, T. Barrick, J. A. Hollingsworth, and V. I. Klimov, Appl. Phys. Lett. **82**, 2793 (2003).
[19]V. I. Klimov, J. Phys. Chem. B **104**, 6112 (2000).
[20]M. A. Petruska, A. V. Malko, P. M. Voyles, and V. I. Klimov, Adv. Mater. (Weinheim, Ger.) **15**, 610 (2003).
[21]V. Klimov and D. McBranch, Phys. Rev. Lett. **80**, 4028 (1998).
[22]V. I. Klimov, A. A. Mikhailovsky, D. McBranch, C. Leatherdale, and M. G. Bawendi, Science **287**, 1011 (2000).
[23]H. Htoon, J. A. Hollingsworth, R. Dickerson, and V. I. Klimov, Phys. Rev. Lett. **91**, 227401 (2003).
[24]H. Htoon, J. A. Hollingsworth, A. V. Malko, R. Dickerson, and V. I. Klimov, Appl. Phys. Lett. **82**, 4776 (2003).
[25]M. A. Hines and P. Guyot-Sionnest, J. Phys. Chem. **100**, 468 (1996).
[26]X. G. Peng, M. C. Schlamp, A. V. Kadavanich, and A. P. Alivisatos, J. Am. Chem. Soc. **119**, 7019 (1997).
[27]S. Kim, B. Fisher, H.-J. Eisler, and M. G. Bawendi, J. Am. Chem. Soc. **125**, 11466 (2003).
[28]L. P. Balet, S. A. Ivanov, A. Piryatinski, M. Achermann, and V. I. Klimov, Nano Lett. **4**, 1485 (2004).
[29]S. A. Ivanov, J. Nanda, A. Piryatinski, M. Achermann, L. P. Balet, I. V. Bezel, P. O. Anikeeva, S. Tretiak, and V. I. Klimov, J. Phys. Chem. B **108**, 10625 (2004).
[30]M. A. Hines and P. Guyot-Sionnest, J. Phys. Chem. B **102**, 3655 (1998).
[31]V. I. Klimov and D. McBranch, Opt. Lett. **23**, 277 (1998).
[32]V. I. Klimov, Ch. J. Schwartz, D. W. McBranch, C. A. Leatherdale, and M. G. Bawendi, Phys. Rev. B **60**, 13740 (1999).
[33]V. I. Klimov, in *Semiconductor and Metal Nanocrystals: Synthesis and Electronic and Optical Properties*, edited by V. I. Klimov (Marcel Dekker, New York, 2004), p. 159.
[34]V. I. Klimov, Ch. J. Schwartz, D. W. McBranch, C. A. Leatherdale, and M. G. Bawendi, Phys. Rev. B **60**, R2177 (1999).
[35]A. V. Malko, A. A. Mikhailovsky, M. A. Petruska, J. A. Hollingsworth, and V. I. Klimov, J. Phys. Chem. B **108**, 5250 (2004).
[36]A. A. Mikhailovsky, A. V. Malko, J. A. Hollingsworth, M. G. Bawendi, and V. I. Klimov, Appl. Phys. Lett. **80**, 2380 (2002).
[37]D. Katz, T. Wizansky, O. Millo, E. Rothenberg, T. Mokari, and U. Banin, Phys. Rev. Lett. **89**, 086801 (2002).
[38]V. C. Sundar, H.-J. Eisler, and M. G. Bawendi, Adv. Mater. (Weinheim, Ger.) **14**, 739 (2002).